# Multi-band polarization switch based on magnetic fluid filled dual-core photonic crystal fiber

Lianzhen Zhang(张连震), Xuedian Zhang(张学典)†, Xiantong Yu(俞宪同), Xuejing Liu(刘学静), Jun Zhou(周军), Min Chang(常敏), Na Yang(杨娜), and Jia Du(杜嘉)

*Key Laboratory of Optical Technology and Instrument for Medicine, Ministry of Education, University of Shanghai for Science and Technology, Shanghai* 200093, *China*

(Received 7 August 2022; revised manuscript received 4 October 2022; accepted manuscript online 14 October 2022)

The research of high-performance polarization controllers is of great significance for expanding the application field of polarization optics. Here, a polarization switch is demonstrated by using a dual-core photonic crystal fiber (DCPCF) with four symmetrical air holes, placed above and below each core, filled with magnetic fluid (MF). The switch, which utilizes a magnetic field to change the coupling length ratio of the *x* and *y* polarization modes, enables dynamic tuning of the polarization state and extinction ratio. Numerical results show that when the working length is 36.638 mm, the magneto–optical polarization switch can operate in four communication bands, *i.e.*, 1509 nm to 1520 nm, 1544 nm to 1556 nm, 1578 nm to 1591 nm, and 1611 nm to 1624 nm. Moreover, the extinction ratio (ER) is greater than 20 dB in the fiber length range of 38.5 mm to 38.7 mm, indicating that the device has a good fault tolerance for the interception of the fiber length.

**Keywords:** polarization switch, magnetic fluid, dual-core photonic crystal fiber

**PACS:** 42.25.Ja, 42.81.–i, 42.81.Gs, 42.81.Wg **DOI:** 10.1088/1674-1056/ac9a37

## 1. Introduction

As an electromagnetic wave, light possesses several basic characteristics, which include phase, intensity, polarization, and wavelength.[1] Since the polarization characteristic is a vector with multi-dimensional characteristics, its regulation requires more advanced devices.[2] In recent years, with the improvement of the ability to control the polarization characteristics of light, the unique advantages of polarization optical methods are attracting more attention. Nowadays, polarized optics has been widely used in the fields of optical communication, optical sensing and biomedicine.[2–4] In order to further tap the potential of polarized light methods, the control of light polarization state is still a current research hotspot. At present, the polarization state of light in space is mainly controlled by birefringent elements, such as polarization splitting prism, thin-film polarization beam splitters (PBS), and wave plates.[5,6] For the development of integrated photonics, controlling the polarization state of light in silicon-based waveguides is of great significance. Many silicon-based waveguide PBS and rotators with excellent performance have been reported.[7,8] With the increasing application of optical fibers in modern optical systems, it is of great significance to study the polarization controllers based on optical fibers. At present, there have been many reports on the research of fiber PBS and fiber polarization filter,[9–15] but there are still some deficiencies in these reports. Firstly, the cost of introducing elliptical holes or inconsistent round holes to increase birefringence is that it will be a great challenge to fabricate fibers. The coexistence of different shapes holes is challenging in photonic crystal fiber (PCF) manufacturing.[16] Then, in pursuit of structural miniaturization, its compatibility with conventional fiber systems is ignored. Finally, the device cannot convert the polarization state of the output modes. In addition, there are few reports on all-fiber polarization switch.

Recently, we have witnessed the rapid development of high-performance all-fiber devices in the PCF platforms, combining with different optoelectronic materials, such as metals,[17–19] two-dimensional materials,[20–22] and liquids,[23–25] to achieve different functions. The cladding of PCF is composed of regularly arranged air holes, which facilitate the combination of PCF with different optoelectronic materials. PCF, filled with functional materials, will exhibit different light guiding properties. Optical fiber sensing,[26] light modulators,[25,27] *etc*. can be designed according to the principles. The combination of magnetic fluid (MF) and PCF, by full or selective filling, has attracted widespread attention. Many related devices have been reported, such as magnetic field sensors,[28–30] magneto–optical modulators,[31] and magneto–optical isolators.[32]

In this paper, we proposed a polarization switch based on dual-core photonic crystal fiber (DCPCF) with same diameter cladding air holes, and analyzed its characteristics with magnetic field or not, respectively. The result shows that, in a free magnetic condition or its strength is less than a critical value, it can be used as a PBS. However, when the value is more than the critical value, the power of the received polarization mode

†Corresponding author. E-mail: xdzhang@usst.edu.cn

© 2023 Chinese Physical Society and IOP Publishing Ltd 

decreases or increases at out ports. Therefore, the extinction ratio (ER) of the output polarization mode can be ameliorated by adjusting the magnitude of the magnetic field, and the polarization state can be rotated under a certain magnetic field magnitude. In addition, we analyzed the influence of the fiber length interception on the performance of the device. The results show that the switch has a good fault tolerance for the interception of the fiber length.

## 2. Model and theory

Figure 1 shows the schematics illustration of the polarization controller based on DCPCF with uniform circular holes. The air holes in the cladding of the PCF are periodically arranged in a hexagonal shape, the diameter of all the air holes is $d$, and the distance between the two holes is $\Lambda$. Two cores, C1 and C2, are formed by removing two air holes from the periodically arranged air holes. The base material of the PCF is silica, and its dispersion model can be described by the Sellmeier equation.[33] The eight holes, painted in blue in Fig. 1, are filled with MF. When there is no magnetic field around the MF or the magnetic field magnitude is lower than its $H_c$, the refractive index of the MF does not change. However, when the surrounding magnetic field magnitude exceeds $H_c$, the refractive index can be changed by adjusting the magnitude of the magnetic field. The relationship between the refractive index of the MF and the strength of the magnetic field can be described by the Langevin function[34,35]

$$n_{\mathrm{MF}} = (n_{\mathrm{s}} - n_{\mathrm{o}}) \left[ \coth\left( \alpha \frac{H - H_{\mathrm{c}}}{T} \right) - \frac{T}{\alpha (H - H_{\mathrm{c}})} \right] + n_{\mathrm{o}} \quad (\text{for } H > H_{\mathrm{c}}), \tag{1}$$

where $n_{\mathrm{o}}$ is the refractive index of the MF when the ambient magnetic field strength is less than $H_{\mathrm{c}}$, $n_{\mathrm{s}}$ is the saturation refractive index of the MF. $H$ and $T$ are the magnetic field strength (in unit Oe, 1 Oe = 79.5775 A·m$^{-1}$) and temperature (in unit K) of the environment, respectively, and $\alpha$ represents the fitting parameters. In this paper, a water-based MF with a particle volume concentration of 0.53 emu/g was used, and $H_{\mathrm{c}}$ and $T$ is assumed 43 Oe and 294 K, respectively.[15]

Combining mode coupling theory and super-mode theory,[36] when the DCPCF is viewed as a monolithic waveguide, each mode in the waveguide will form two supermodes, namely the symmetric mode ($y$-even, $x$-even) and the asymmetric mode ($y$-odd, $x$-odd). The coupling law of DCPCF can be analyzed by the superposition of supermodes when the light with the energy of $P_{\mathrm{in}}$ is input from the core C1. The most energy is transferred to C2 when the phase difference between the symmetric and antisymmetric modes is $\pi$. The two cores in the DCPCF are identical, so the phase matching condition is satisfied. Theoretically, the complete coupling of energy can be achieved, and the coupling distance is $L_{x,y}$,

$$L_{x,y} = \frac{\pi}{\beta_{\mathrm{s}}^{x,y} - \beta_{\mathrm{a}}^{x,y}}, \tag{2}$$

where $\beta_{\mathrm{s}}^{x,y}$ and $\beta_{\mathrm{a}}^{x,y}$ are the propagation constants of the four supermodes, $\beta = 2\pi n_{\mathrm{eff}}/\lambda$, $n_{\mathrm{eff}}$ is the effective refractive index, and $\lambda$ is the wavelength in free space. Assuming the light is input in C1, then the normalized energy of $x$ or $y$ polarization mode output by C1 is given by

$$\eta_{\mathrm{C1-out}}^{x,y} = \frac{P_{\mathrm{C1-out}}^{x,y}}{P_{\mathrm{in}}} = \cos^2(\pi z / 2L_{x,y}). \tag{3}$$

To achieve complete separation of $x$- and $y$-polarized light, it is necessary to satisfy the propagation distance $z = mL_x = nL_y$, where $m$ and $n$ are positive integers with different parities. It can be concluded that the device length is determined by the ratio of $L_x$ to $L_y$, which is defined as the coupling length ratio (CLR):

$$\mathrm{CLR} = L_x / L_y = n/m. \tag{4}$$

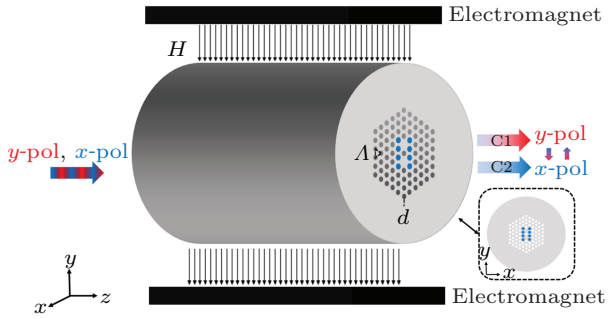



**Fig. 1.** Schematic diagram and cross section of the polarization switch based on DCPCF. When the magnetic field is none or its strength is less than a critical value, the two polarization (pol) modes, $y$-pol (red) and $x$-pol (blue), are split into the two cores at the output ports. When the magnetic field strength is more than the critical value, the ER of the output polarization mode, $y$-pol (red) and $x$-pol (blue), can not only be adjusted with the change of the magnetic field, but also the polarization states can be rotated.

For conventional PBS, the ER is a key parameter to measure its performance. ER is the ratio of the energy of the polarized light to be eliminated in a fiber core at the output port to the obtained. The calculation method is as follows:

$$\mathrm{ER} = 10 \log_{10}\left( \frac{P_{\mathrm{C1-out}}^{x}}{P_{\mathrm{C1-out}}^{y}} \right). \tag{5}$$

The separation of the two polarization modes in the fiber is achieved because of the difference in their coupling distance from one core to the other. The reason for the different coupling distances, however, is their different propagation constants in the fiber. Therefore, it can be known that the polarization state of the beam at the output end can be changed by changing the length of the device or the propagation constant of the polarization modes.

## 3. Analysis and results

### 3.1. Optimization of the fiber structure

In this article, a finite element mode solver (COMSOL) is adopted to optimize the parameters and performance of the DCPCF. Most of the current reports on PBS have introduced irregular air holes, such as elliptical air holes, circular air holes with different diameters, in the cladding of DCPCF. As a result, more parameters need to be analyzed when optimizing the device. The diameters of the air holes in the cladding of the DCPCF designed in this paper are consistent. In this case, we only need to analyze the influence of the air hole arrangement period $\Lambda$ and the duty cycle $d/\Lambda$ on its performance. In addition, this approach can reduce the complexity of the fiber fabrication process compared to using non-uniform pores.

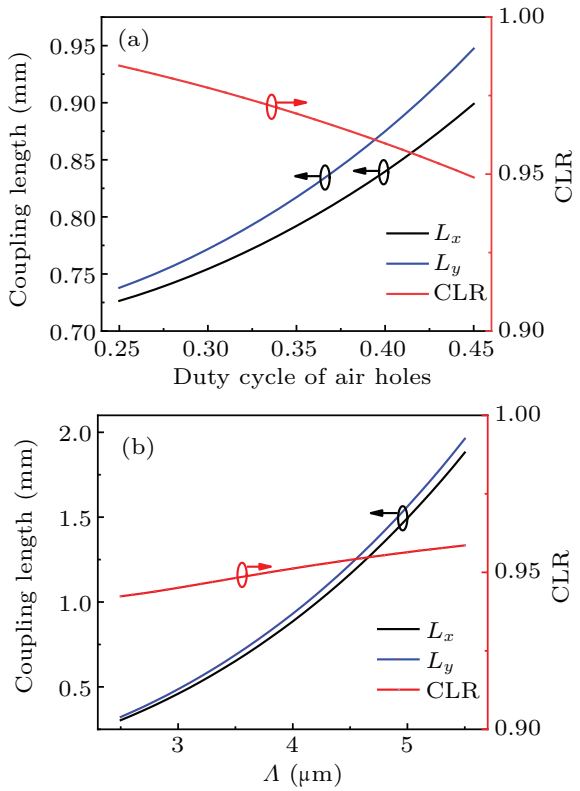



**Fig. 2.** At the wavelength of 1.55 μm: (a) the effect of duty ratio of the air holes on CL and CLR with the parameters of $\Lambda = 4$ μm, (b) the influence of $\Lambda$ on CL and CLR with the parameter of $d/\Lambda = 0.44$.

Figure 2 depicts the influence of duty ratio and the hole spacing on the coupling lengths and CLR. Figure 2(a) shows the effect of duty ratio of the air holes on CL and CLR with the parameter of $\Lambda = 4$ μm. The results show that $L_x$ and $L_y$ increase with the increase of duty cycle, while CLR decreases. Because the coupling length $L_x < L_y$, the smaller the CLR, the shorter the length of the device will be.[10] When the duty cycle in the PCF is less than 0.45,[37] the single-mode transmission with infinite cutoff can be realized, so $d/\Lambda = 0.44$ is set. Figure 2(b) shows that the increase of the air hole spacing also leads to the increase of $L_{x,y}$ when the duty cycle is fixed at $d/\Lambda = 0.44$. Although the CLR also increases, the change is not significant. The above results first show that this method can be used for the modulation of the polarization state. In addition, the results show that after we determine the duty cycle of the air holes, the change of the air hole spacing has little effect on the CLR, which will be beneficial for us to design polarization controllers of various sizes. In order to be compatible with the traditional single-mode fibre communication system, $\Lambda = 5.25$ μm.

According to the optimized parameters, the device is subjected to mode analysis, and the distribution of transmission modes ($y$-even, $y$-odd, $x$-even, and $x$-odd) of the device at a wavelength of 1550 nm is obtained as shown in Fig. 3. The electric field of the even mode is in the same direction (symmetric mode), and the direction of the odd mode is opposite (asymmetric mode). After analysis, both the even and odd modes of the $x$ and $y$ polarization modes have energy leakage into the MF-filled holes, but more than 85% of the energy is still confined in the core. Since the refractive index of the MF is higher than that of air, it is more likely to cause energy leakage into the fiber cladding. Confinement loss can be used to measure the PCF's ability to confine light. A perfectly matched layer is introduced into the numerical model to analyze the confinement loss of DCPCF. The results show that the confinement loss of the modes supporting transmission in the DCPCF of the entire communication band is less than $10^{-8}$ dB/m, which is negligible for millimeter-level device.

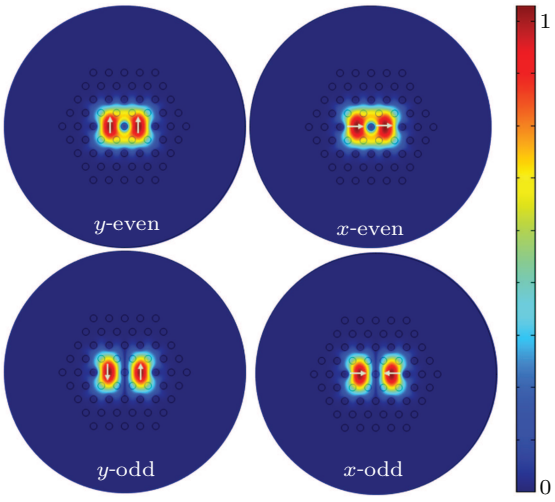



**Fig. 3.** Mode field distribution of supermodes in DCPCF, at $\lambda = 1550$ nm, $\Lambda = 5.25$ μm, $d/\Lambda = 0.44$.

### 3.2. Characteristics of the polarization beam splitter

The PBS performance of DCPCF in the absence of magnetic field was analyzed. When the incident light is incident from the fiber core C1, the energy of the two polarization modes in the two fiber cores changes as the propagation distance increases, and finally only one polarization state of light can be obtained in each fiber core. According to formula (3), the normalized power of the two polarization states

in C1 can be obtained as a function of the transmission distance, at $\Lambda = 5.25$ μm, $d/\Lambda = 0.44$, $\lambda = 1550$ nm. As shown in Fig. 4, when incident at C1, the normalized powers of the two polarization modes at the output of C1 vary with different periods. When the length of the fiber is 38.638 mm, the main energy at the output end of C1 is *y* polarization mode, and the energy in the *x* polarization mode almost does not exist, thus realizing the function of polarization beam splitting. The ER is −88.6 dB, which is another important indicator for PBS. The results show that the device has excellent splitting function when no external magnetic field is applied.

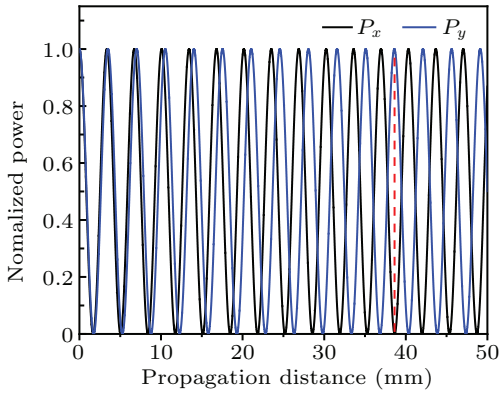



**Fig. 4.** The normalized power of *x* and *y* polarizations *versus* the transmission distance, at $\lambda = 1550$ nm, $\Lambda = 5.25$ μm, $d/\Lambda = 0.44$. The red dotted line is magnetic field magnitude at the first order separate length of 38.638 mm.

### 3.3. Analysis of magnetic tuning characteristics

After the dimensions of the device are determined, the factors that affect $L_x$ and $L_y$ are mainly wavelength and magnetic field magnitude. The propagation constants $\beta$ of the four supermodes in the DCPCF will change with the wavelength, and the coupling distance will also change according to Eq. (2), as shown in Fig. 5(a). In the wavelength range of 1260 nm–1675 nm, $L_x$ and $L_y$ decrease as the wavelength increases. In addition, the refractive index of the MF increases with the increase of the magnetic field magnitude, so the change of the magnetic field magnitude will also cause the change of the propagation constant of the four supermodes in the DCPCF. As shown in Fig. 5(b), when the magnetic field strength is lower than the critical value, the coupling distance of the two polarization modes does not change with the change of the magnetic field, but when the magnetic field magnitude exceeds the critical value, it will decrease with the increase of the magnetic field magnitude. Furthermore, the rate of change of the coupling distance decreases with increasing magnetic field magnitude. This is because the rate of change of the refractive index of the magnetic fluid decreases as the magnetic field magnitude increases, eventually reaching its saturation value.

The normalized power and ER for the *x* and *y* polarization modes at the outports vary with wavelength. Combining Eqs. (3) and (5), the function curve of the normalized energy and ER of the *x* and *y* polarization modes of the output port of the fiber core C1 as a function of wavelength can be drawn without magnetic field, as shown in Fig. 6. As described in the figure, the change of wavelength will cause the change of the energy and ER of the two polarization modes at the same side output port under the condition of fixed device structure. This is because a change in wavelength causes a change in the coupling lengths $L_x$ and $L_y$, which have been analyzed in detail above. As shown in Fig. 6, at the wavelengths of 1514 nm, 1550 nm, 1585 nm, and 1618 nm, the normalized energy and ER are relatively high, and their values are (98.97%, 37.5 dB), (99.87%, −88.7 dB), (99.72%, 37.9 dB), (98.95%, −39.7 dB), respectively, the positive ER means that the main energy is *x*-polarization mode, and the negative ER means that the main energy is in the *y*-polarization mode. The magnetic tuning characteristics of the device are analyzed below.

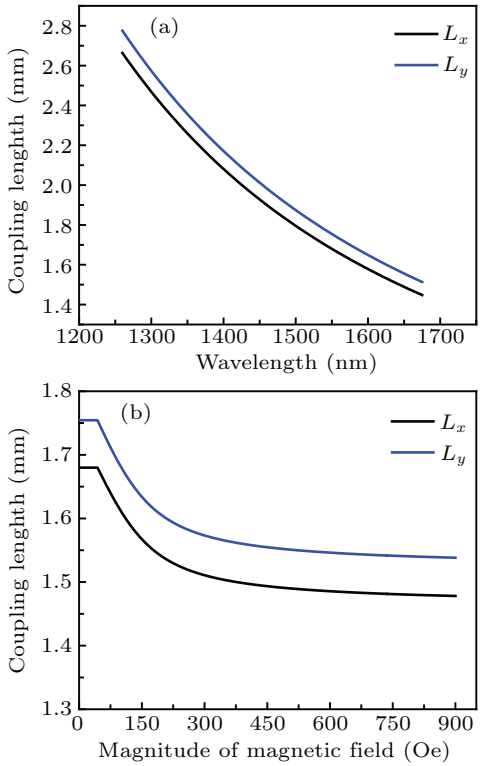



**Fig. 5.** Coupling length *versus* the magnitude of (a) wavelength and (b) magnetic intensity, at $\lambda = 1550$ nm, $\Lambda = 5.25$ μm, $d/\Lambda = 0.44$.

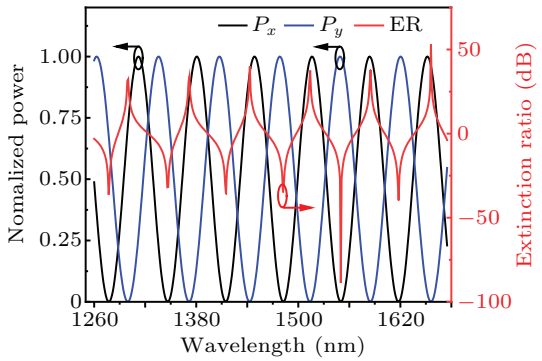



**Fig. 6.** The extinction ratio and normalized power *versus* the wavelength without magnitude of magnetic field, at $z = 38.638$ mm, $\Lambda = 5.25$ μm, $d/\Lambda = 0.44$.

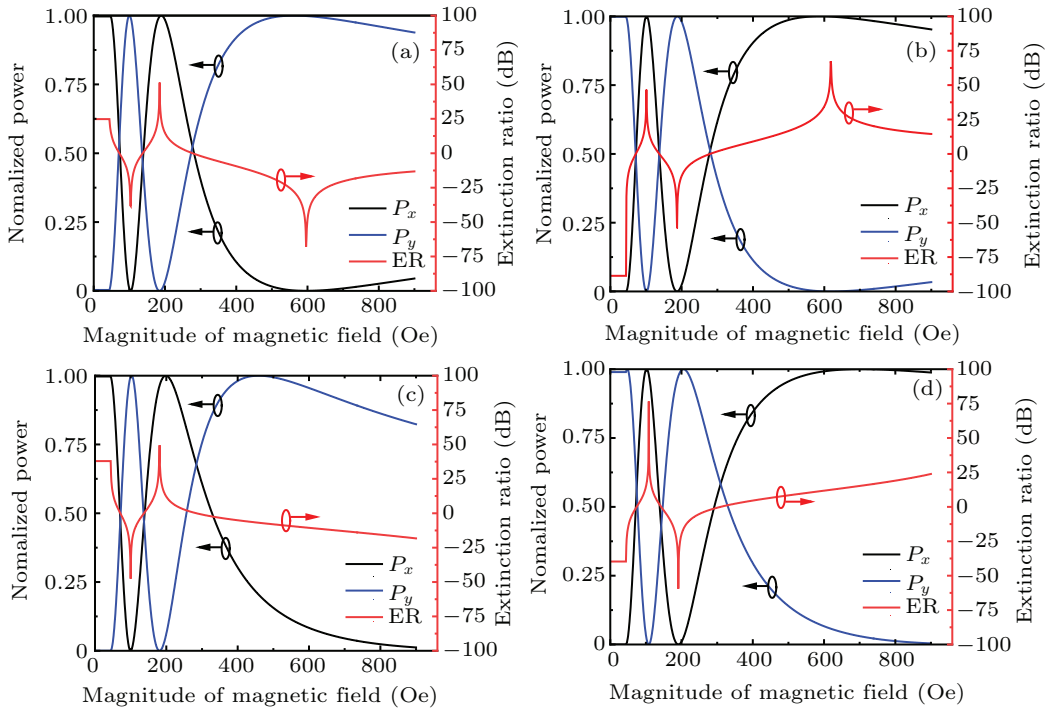



**Fig. 7.** Normalized power and extinction ratio *versus* the magnitude of magnetic field at different wavelengths (a) 1514 nm, (b) 1550 nm, (c) 1585 nm, (d) 1618 nm.

Figure 7 depicts the normalized power and ER for the two polarization modes of the C1 output port as a function of magnetic field amplitude. According to formula (1), it can be known that the refractive index of MF does not change when the magnetic field $H < 44$ Oe, which does not affect the change of the intensity of the two polarization modes of the outports. As shown in Fig. 7, the intensity and ER of the two polarization modes at the output port are stable in the range of 0 Oe–43 Oe. When the magnetic field intensity $H > 44$ Oe, the refractive index of MF changes with the magnetic field intensity, which will affect the intensity of the two polarization modes of the output port. Figure 7(a) illustrates the normalized energy and ER at the wavelength of 1514 nm. The results show that the normalized energy and ER, at magnetic fields of 103 Oe, 184 Oe, 596 Oe, are (99.5%, 38.03 dB), (99.52%, 38.84 dB), (99.85%, 67.92 dB), respectively. At the wavelength of 1550nm, the results are shown in Fig. 7(b). The normalized energy and ER of the two polarization modes, at magnetic fields of 101 Oe, 187 Oe, 618 Oe, are (99.98%, 46.6 dB), (99.98%, 54.04 dB), (99.89%, 67.29 dB), separately. Figure 7(c) demonstrates the normalized energy and ER at the wavelength of 1585 nm. The results show that the normalized energy and ER, at magnetic fields of 100 Oe, 181 Oe, are (99.62%, 47.57 dB), (96.4%,49.46 dB), respectively. At the wavelength of 1618 nm, the results are shown in Fig. 7(d). The normalized energy and ER of the two polarization modes, at magnetic fields of 108 Oe, 191 Oe, are (98.07%, 76.56 dB), (97.51%, −59.44 dB), separately.

The positive ER means that the main energy is in the *x*-polarization mode, and the negative ER means that the main energy is in the *y*-polarization mode. It can be concluded that the rotation of the polarization mode of the output port can be realized by changing the amplitude of the magnetic field, and the ER of the output polarization mode can also be tuned by the magnetic field. The device can achieve polarization mode rotation at the first-order polarization separation length. When the magnetic field magnitude is 103 Oe, 101 Oe, 100 Oe, and 108 Oe, respectively, the polarization rotation at wavelengths of 1514 nm, 1550 nm, 1585 nm, and 1618 nm can be achieved. In this case, figure 8 depicts the wavelength as a function of ER when outputting *x* or *y* polarization modes for different wavelengths. Since the device needs to output different polarization modes at the same wavelength, the ER when outputting the *x* and *y* polarization modes separately should be more than 10 dB. In this case, when the central wavelengths are 1514 nm, 1550 nm, 1585 nm, and 1618 nm, the wavelength ranges that satisfy the above conditions are 1509 nm–1520 nm, 1544 nm–1556 nm, 1578 nm–1591 nm, and 1611 nm–1624 nm, respectively.

The above analysis results are obtained at the temperature of 21 °C. However, when the ambient temperature changes, the characteristics of the MF will also be affected. Thus, the influence of temperature on the device performance should be considered. The variation of temperature not only affects the refractive index of the MF, but also changes its critical magnetic field strength $H_c$.[35,38] In the literature, the influence of temperature on the refractive index and $H_c$ of water-based MF with a concentration of 0.85 emu/g was analyzed. The critical $H_c$ was found to increase from 22 Oe to 50 Oe upon in-

creasing the temperature from 8.0 °C to 60.0 °C, and it can be seen that $H_c$ and temperature are basically linear. In addition, they found that the refractive index of the MF increases linearly and continuously with the particle concentration under zero field, and the magnitude of thermo–optic coefficient $dn_{MF}/dT$ is less than $10^{-4}$ °C$^{-1}$. The concentration of the water-based MF used in this paper is 0.53 emu/g.[39] Therefore, its characteristics will have a similar variation trend as the MF with a concentration of 0.85 emu/g. The above analysis indicates that the alteration of temperature will change the magnetic field strength of the polarization switch for polarization conversion to a certain extent.

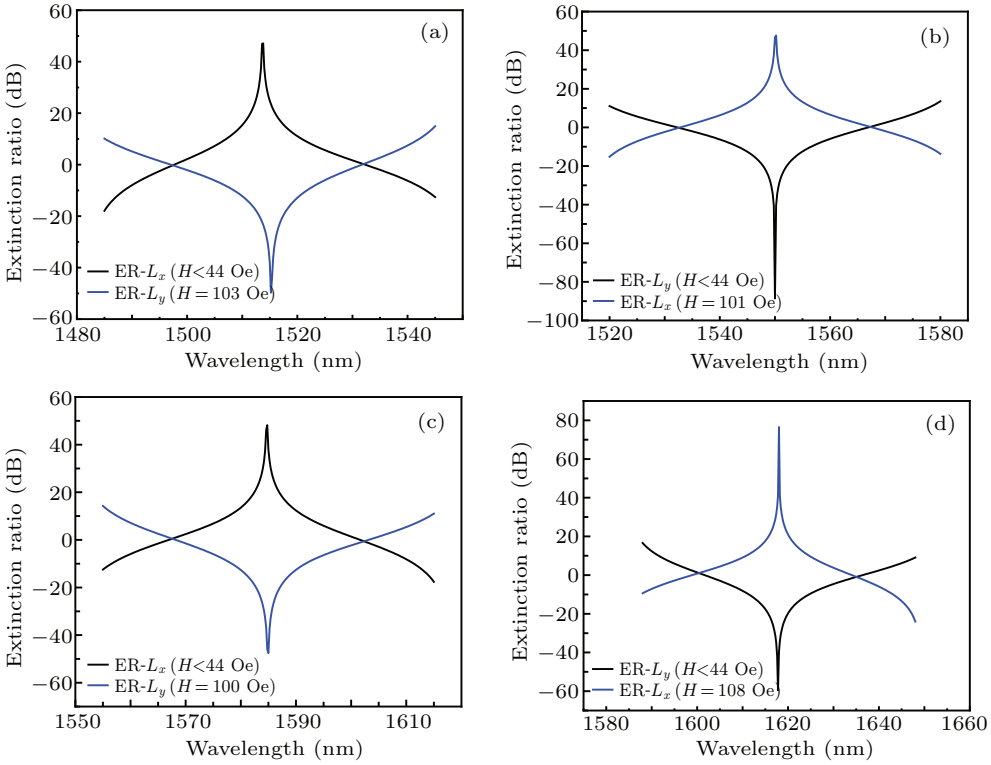



**Fig. 8.** Extinction ratio of *x* or *y* polarization mode *versus* the wavelength, at the centre wavelength of (a) 1514 nm; (b) 1550 nm; (c) 1585 nm; (d) 1618 nm.

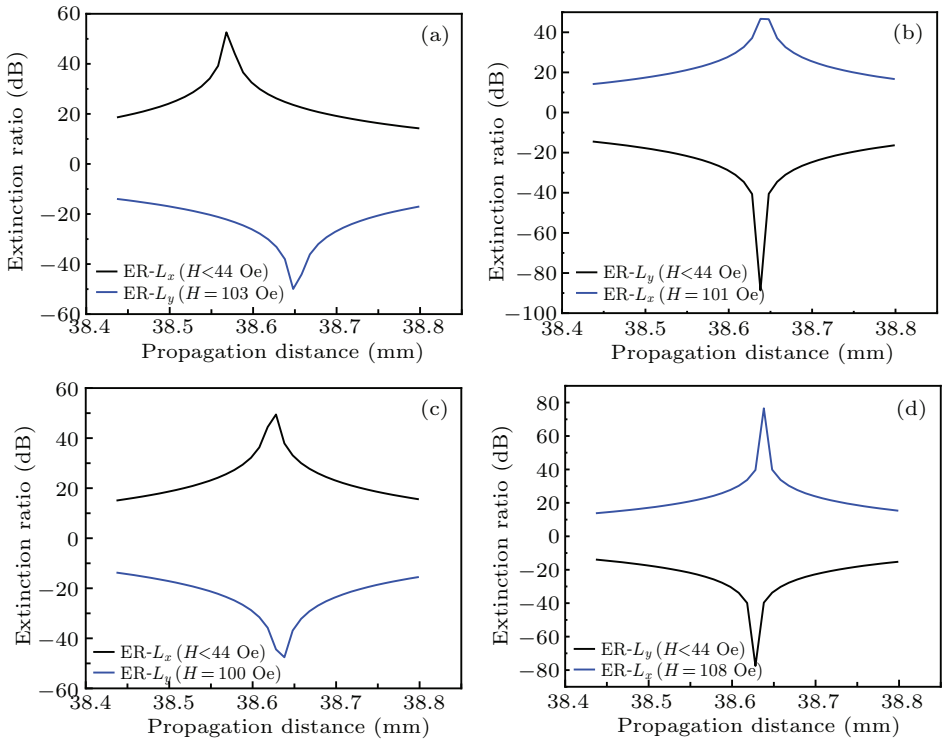



**Fig. 9.** Extinction ratio of *x* or *y* polarization mode *versus* the intercepted fibre length, at different wavelengths of (a) 1514 nm, (b) 1550 nm, (c) 1585 nm, (d) 1618 nm.

The fiber length of the polarization controller designed in this paper is 38.638 mm. At the central wavelength, as a PBS, the ER are 24.79 dB, −88.65 dB, 37.89 dB, and 39.69 dB, respectively, and the ER when the polarization rotation occurs are −38.03 dB, 46.67 dB, −47.57 dB, and 76.56 dB. This length can be precisely controlled when analyzing its characteristics by numerical simulation. However, there is an error when cutting the fiber in the experiment. Figure 9 depicts the curves of the ER as a function of the cutoff length of the fiber when the wavelengths are 1514 nm, 1550 nm, 1585 nm, and 1618 nm, respectively. As shown in the figure, the absolute value of the extinction ratio between the lengths of 38.5 mm and 38.7 mm is greater than 20 dB, which indicates that the device has a good fault tolerance for the interception of the fibre length.

## 4. Conclusion

In conclusion, we have conducted a detailed study of a novel polarization switch based on DCPCF, whose cladding air holes are uniform in diameter. The DCPCF is infiltrated with MF in the four holes longitudinal symmetrically of each core. Firstly, the influence of structural parameters on the performance of the polarization controller is analyzed by the full vector finite element method. The results show that the working length of the controller is 38.638 mm. The operating bands with ER greater than 10 dB when outputting $x$ or $y$ polarization modes include 1509 nm to 1520 nm, 1544 nm to 1556 nm, 1578 nm to 1591 nm, and 1611 nm to 1624 nm. The magnetic magnitudes for polarization rotation in these bands are 103 Oe, 101 Oe, 100 Oe, and 108 Oe, respectively. The ER of the output $x$ or $y$ polarization is greater than 20 dB in a range of 38.5 mm to 38.7 mm for the proposed polarization controller. It shows that the device has a good tolerance for the fiber cut length. In addition, the polarization controller has the characteristics of simple manufacture and fair compatibility with traditional optical fiber communication and sensing systems.

## Acknowledgement

Project supported by the National Key Research and Development Program of China “National Quality Infrastructure” (Grant No. 2021YFF0600902).

## Data availability

Data underlying the results presented in this paper may be available from the corresponding author upon reasonable request.

## References

[1] Huard S 1997 *Polarization of light* (Wiley-VCH) p. 348
[2] He C, He H, Chang J, Chen B, Ma H and Booth M J 2021 *Light: Sci. Appl.* **10** 194
[3] Huang C P, Wang Q J, Yin X G, Zhang Y, Li J Q and Zhu Y Y J A O M 2014 *Adv. Opt. Mater.* **2** 723
[4] Li J, Chen S, Yang H, Li J, Yu P, Cheng H, Gu C, Chen H T and Tian J 2015 *Adv. Funct. Mater.* **25** 704
[5] L B *JOSA*, p. 665
[6] Schledermann M and Skibowski 1971 *Appl. Opt.* **10** 321
[7] Chen Z, Yang J, Wong W H, Pun E Y B and Wang C 2021 *Photon. Res.* **9** 2319
[8] Sun C, Yu Y, Ding Y, Li Z, Qi W and Zhang X 2020 *Photon. Res.* **8** 978
[9] Chen N, Zhang X, Lu X, Zhang Z, Mu Z and Chang M 2020 *Micromachines* **11** 706
[10] Zhang X, Liu Z, Gui Y, Gan H, Guan Y, He L, Wang X, Shen X and Dai S 2021 *Opt. Express* **29** 39601
[11] Wang J, Pei L, Weng S, Wu L, Li J and Ning T 2018 *Appl. Opt.* **57** 3847
[12] Zi J, Li S, An G and Fan Z 2016 *Opt. Commun.* **363** 80
[13] Shuo L, Shu-Guang L and Ying D 2012 *Opt. Laser. Technol.* **44** 1813
[14] Hu W, Yang N, Wu L, Cheng P, Cheng S, Hu X, Li Q, Zhou A, Yang M and Guo D 2022 *J. Lightwave Technol.* **40** 2128
[15] Wang J, Pei L, Weng S, Wu L, Huang L, Ning T and Li J 2017 *J. Lightwave Technol.* **35** 2772
[16] Issa N A, van Eijkelenborg M A, Fellew M, Cox F, Henry G and Large M C 2004 *Opt. Lett.* **29** 1336
[17] Wang Y, Li S, Li J, Guo Y and Wang M 2021 *J. Lightwave Technol.* **39** 1791
[18] Yan X, Guo Z, Cheng T and Li S 2020 *Opt. Laser. Technol.* **126** 106125
[19] Chen N, Chang M, Zhang X, Zhou J, Lu X and Zhuang S 2019 *Nanomaterials* **9** 1587
[20] Cheng X, Zhou X, Tao L, Yu W, Liu C, Cheng Y, Ma C, Shang N, Xie J and Liu K 2020 *Nanoscale* **12** 14472
[21] Chen J H, Xiong Y F, Xu F and Lu Y Q 2021 *Light: Sci. Appl.* **10** 1
[22] Yu X, Yuan Y, Xu J, Yong K T, Qu J and Song J 2019 *Laser Photon. Rev.* **13** 1800219
[23] Dai Z F, Jiang W F, Wang L, Chen M Y, Gao Y F and Ren N E 2019 *Acta Phys. Sin.* **68** 084206 (in Chinese)
[24] Mitu S A, Kumar K V, Mollah M A, Mishra S, Ahmed K, Bui F M and Al-Zahrani F A 2022 *IEEE Trans. Nanotechnol.* **21** 90
[25] Huang Y, Wang Y, Zhang L, Shao Y, Zhang F, Liao C and Wang Y 2019 *J. Lightwave Technol.* **37** 1903
[26] Zhang C, Pu S, Hao Z, Wang B, Yuan M and Zhang Y 2022 *Nanomaterials* **12** 862
[27] Tian S, Yang T, Zhang J, Xie K, Ma J, Hong L, Luo Y and Hu Z 2021 *J. Lightwave Technol.* **39** 3297
[28] Li X, Ma R and Xia Y 2018 *J. Lightwave Technol.* **36** 1620
[29] Liu Q, Xing L and Wu Z 2019 *Opt. Commun.* **452** 238
[30] Gao T, Ma G, Wang Y, Gao D, Qin W, Wangb Y and Yan C 2022 *IEEE Sens. J.* **22** 4022
[31] Horng H E, Chieh J J, Chao Y, Yang S Y, Hong C Y and Yang H C 2005 *Opt. Lett.* **30** 543
[32] Saker K, Lahoubi M and Pu S 2021 *J. Comput. Electron.* **20** 1326
[33] Malitson I H 1965 *JOSA* **55** 1205
[34] Hong C Y, Yang S Y, Horng H E and Yang H C 2003 *J. Appl. Phys.* **94** 3849
[35] Chen Y, Yang S Y, Tse W, Horng H E, Hong C Y and Yang H C 2003 *Appl. Phys. Lett.* **82** 3481
[36] Liu J M 2005 *Photonic Devices* (Cambridge, UK: Cambridge University) pp. 164–210
[37] Mortensen N A 2002 *Opt. Express* **10** 341
[38] Hong C Y, Horng H E and Yang S Y 2004 *Phys. Stat. Sol.* **1** 1604
[39] Gao R, Jiang Y and Abdelaziz S 2013 *Opt. Lett.* **38** 1539